A High Rate SMA Actuator for Aerodynamic Load Control on Wind Turbines

A. Lara-Quintanilla, A.W. Hulskamp, H.E.N. Bersee

Faculty of Aerospace Engineering, Delft University of Technology, Delft, The Netherlands

Abstract: This paper discusses the development of a high rate shape memory alloy (SMA) driven actuator. The concept of the actuator was developed to act as aerodynamic load control surface on wind turbines. It was designed as a plate or beam-like structure with prestrained SMA wires embedded off its neutral axis. Moreover, the SMA material was embedded in channels through which air was forced to actively cool the wires when the recovery load was to be released. Wires were implemented on both sides of the neutral axis to deflect the beam in both directions.
Thermal analysis of the cooling channels showed that they increased the cooling up to tenfold in comparison to the same set-up without forced convection. Subsequently a fuzzy logic controller was designed to control the thermo-mechanical system. The inputs were the error between the deflection and the set point, the value of the set point and the time derivative of the set point. The output consisted of two signals to the valves that controlled the flow through the channels and a signal heating signal that was split to both sets of wires, depending on its sign. The controller was tested on an antagonistic set-up, through which a similar thermo-mechanic behaviour as with the actuator was obtained, but eliminating the beam dynamics. The results were satisfactory; an actuation bandwidth of 1Hz was attained.
Subsequently, the controller was tested on the actuator. With increasing actuation frequency, until 0.6Hz a relatively small error between the set point and the actual deflection was observed. Above that frequency the error increased, but also the sinusoidal response was lost. This is believed to be due to snap-through behaviour around the neutral position of the actuator. This was substantiated by the apparent inability of the actuator to track the set point around the neutral position in tracking a composite sinusoidal set point.

INTRODUCTION

Within the wind turbine community there has been a large research effort into so called smart rotors over the last decade; rotors that are able to control the aerodynamic loading along the span of the blade (Buhl et al., 2005, Joncas et al., 2005, Basualdo, 2005). The main goal of such a concept is fatigue load reduction because fatigue is one of the largest design drivers for current MW-sized turbines. This will become more important for future, even larger designs. Mit-

igating fatigue loads may therefore lead to lighter rotors or a longer service life. However, this is not possible with current load control systems. Individual Pitch Control (Bossanyi, 2003) might have the potential, but puts a heavy strain on the pitch bearings.
The fatigue loads are induced by a multitude of sources, most of which are related to temporal and spatial variations in inflow, and rotation of the turbine through this varying wind field. The most logical way to counter the main source of these loads is to control the way in which loads are created on the rotor, viz. to control the aerodynamics. But when the aerodynamic loads are controllable, the system could also be used to mitigate loads of a non-aerodynamics nature, such as gravitational and wave loading on off-shore turbines and the dynamic response to transient loads or excitation of certain modes.
There have been many investigations into the feasibility of the concept (van Wingerden et al., 2008), the aerodynamics (Gaunaa, 2010) and control system (Rice and Verhaegen, 2010, van Wingerden, 2008), but an important part of the smart rotor concept is the development of an actuator. Many concepts, using trailing edge devices like micro tabs and synthetic jets, are being pursued, but in this paper the focus is on the deformable trailing edge because it is aerodynamically one of the most effective way of influencing the lift of a spanwise section while maintaining attached flow. For this, several concepts were investigated. Saggere (Saggere and Kota, 1999), for example, developed a mechanism based on distributed compliance driven by a discrete actuator. Also, pneumatically controlled silicone trailing edges are being developed.
Here the embedded adaptive material approach is being investigated. Adaptive materials are very powerful materials for deforming surfaces because they pose a very high power density, they can be embedded dispersed and require little maintenance because there is no wear. In helicopter research, piezo electrics have been mostly implemented for dynamic control (Enenkl et al., 2002, Hall and Prechtl, 1996, Lee and Chopra, 2001) and shape memory alloys (SMA) for quasi static control, so called blade tracking (Singh et al., 2003). However, the requirements for wind turbine blades are different, especially with respect to the required bandwidth and the dimensions of the blade. For instance, a 5MW turbine rotates with a speed of about 0.2Hz and the size of its chord is in the order of meters. The required bandwidth is still unknown because it depends on the specific turbine design, but it has been stipulated that the part of the power spectrum density (PSD) up to three times the rotational frequency constitutes the largest part of the vibration energy. Another bandwidth restriction is posed by the first dynamic eigenmode. Being able to actuate on this frequency will mitigate transient vibrations and could increase the aeroelastic stability. The UpWind reference turbine (Jonkman et al., 2007) was used in this research, of which the 3P frequency is 0.60Hz and the first vibrational mode lies at 0.69Hz. These frequencies are within the theoretical bandwidth of SMA materials but they are only attainable under lab conditions, not when the material is embedded in a plate. In this paper the possibility for a high rate SMA actuated active surface, based on active cooling, will be addressed. This would increase the bandwidth of the embedded SMA into the range required for active control surfaces for wind turbine blades. Apart from actuation frequencies that are in the right range for load control surfaces on wind turbines, additional advantages of basing the actuator on SMA material are its high power density and the large actuation strains (Lagoudas, 2008). The development of the actuator was car-

ried out in four major stages 1) Design and manufacturing of an actuator with internally mounted SMA wires 2) characterisation of the thermal behaviour, 3) development of the controller, to be able to test the system's behaviour 4) Testing the performance of the actuator-controller combination.

DESIGN OF A HIGH RATE SMA ACTUATOR

The Concept

The concept of the actuator was to embed SMA wires inside a beam or plate-like structure inside channels. The SMA wires are previously prestrained and try to recover their original length upon heating them. If the wires are restrained they exert a force on the actuator during the recovery process. Shu (Shu et al., 1997) modeled and tested a flexible cantilever beam bended by externally attached SMA wires at both sides of the beam. However, embedding the wires in the beam to be bent is more convenient for certain applications. There are two manners of eccentric embedding SMA wires into a plate for actuation purposes: direct embedding the SMA wires, what means that they are bonded to the host material, and indirect embedding, what means that the SMA wires are placed into sleeves or channels along the host material and therefore they must be attached to it by means of a gripping system. Zhou (Zhou and Lloyd, 2009) reported that the manufacturing process of directly embedded SMA wires is complex and challenging because controlling the SMA behaviour during curing is difficult. Debonding problems between the wires and the host material have been also observed (Doran, 1994, Zhou and Lloyd, 2009). Hebda (Hebda et al., 1995) simplified the procedure by using two-way shape memory effect wires, although they observed void growth in the host composite material around the Nitinol wires which in turn contributed to a lack of bonding at the interface between the SMA and the composite material. On the other hand, indirectly embedded wires can be placed in the actuator once it is manufactured. Song (Song et al., 2000) used this method to secure Nitinol wires within a honeycomb-cored composite beam for precision position control. In this work, indirectly embedded SMA wires were placed into channels along the beam. This method presents some advantages, amongst others, the manufacturing process is simplified and the wires can be put and replaced easily.

The channels are placed out of the neutral axis of the actuator and the wires are placed on the most outer part of the channel. In this way, a force exerted by the wire results in the highest attainable bending moment on the actuator, and thus in the largest curvature. The wires are mechanically constrained at their ends. Through the channels air - or any other fluid - can be forced to cool the wires at a high rate. The incorporation of the channels requires a certain thickness of the actuator. To limit the bending stiffness of the actuator, it is constructed from pure polymer. The Young's modulus is much lower than reinforced plastics and it has a high level of formability.

Two sets of wires are implemented; one on each side of the actuator. See Figure 1. Controlling the actuator therefore requires two heating and two cooling signals. There are two reasons for this approach. Firstly, this makes it possible to deflect the actuator in both directions. Secondly, in this configuration - called an antagonistic configuration- the wires work against each other.

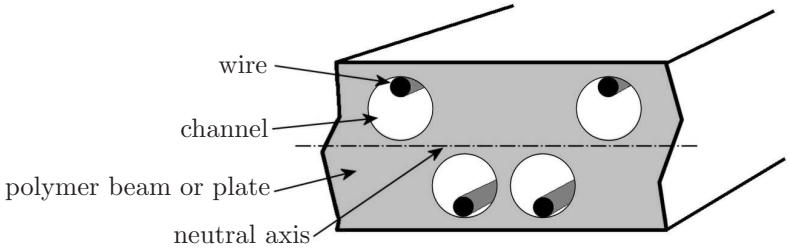

Figure 1: Schematics of a unit cell of the actuator concept.

With one-way shape recovery, a bias force is needed to regain the prestrain of the wire after it is heated. In the case of this actuator a large part of the bias force is formed by the elasticity of the actuator itself, but in an antagonistic configuration one wire generates a (controllable) bias force for the other one. See Figure 2 for a schematic representation of a pure antagonistic set-up and the equivalent of the actuator configuration.

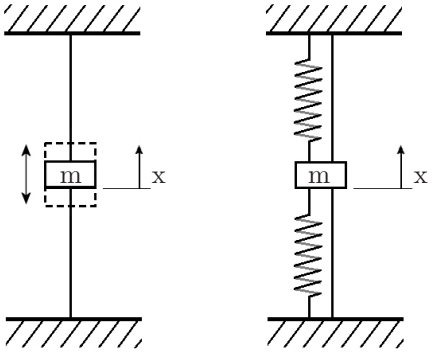

Figure 2: Schematic representation of an antagonistic configuration (left) and for the actuator (right).

In fact, the strain in the actuator is relatively small, as compared to typical actuation strains of the SMA material (Lagoudas, 2008). Therefore the springs in Figure 2 are very stiff and the SMA behaviour almost reduces to so called restrained recovery. The configuration also allows for faster position control because the second wire can be heated while the first one is still cooling down. Normally this poses a disadvantage of the antagonistic configuration because, if both wires are heated in alternating manner, but the cooling capacity is not sufficient, the actuator might become unstable due to the build-up of heat in both sets of wires. With the actuator discussed here, the cooling rate of the wire that is cooling down is increased because of the flow through cooling channels, limiting simultaneous heating of both sets of wires.

Detailing and Manufacturing

To obtain a plate or beam with narrow, straight channels, silicone sleeves were tensioned in a aluminium mould which was filled with a casting resin. After

curing, the sleeves were removed and the product demoulded. Originally, the sleeves were used with electronics as high temperature wire insulation and they had an outer diameter of 1.8mm. Holes were drilled in the casting mould to fit the sleeves through. The fitting was tight enough to prevent leakage of the resin. The holes were placed such that 0.6mm of polymer remains between the channel and the outer surface of the actuator. Since the thickness of the actuator is 6mm, this meant that the whole channel lays on one side of the neutral axis. See Figure 1.
The implemented material system is APA-6, a form of nylon. An advantage of the system is that the properties of the polymer are tuneable to some extent and because the thermoplastic actuator could be welded to other thermoplastic structural elements. Moreover, it's a low cost material.
The whole setup was placed in a hot press and heated to 180°C. The APA-6 casting resin cured with relative low crystallinity at this temperature. See (van Rijswijk, 2007) for details on the material system. This had two advantages. First of all, the modulus of the polymer remained relatively low and thus a flexible actuator was obtained. Secondly, the presence of the amorphous phase made easy removal of the sleeves possible. The resin was cast and left to cure and crystallize for 45min. The mould was cooled down slowly and the sleeves were removed at 70°C because at that temperature there is movement in the amorphous phase. Then, the part was demoulded and the excess resin removed.
The implemented wires were 0.4mm diameter SmartFlex wires from Saes Getters (SAES Smart Materials, New Hartford, NY, USA). The maximum attainable stroke is 5.5%, austenite start temperature is 85°C and martensite finish temperature is 65 °C when the material is loaded at 200 MPa. The fatigue life is longer than 200,000 cycles and the permanent plastic deformation accumulated after 120,000 cycles is 0.3% of the length (Fumagalli et al., 2009). These characteristics make these SMA wires suitable for the current application.
The diameter was chosen to obtain a good balance between force and obtainable cooling rate. Large diameter wires can exert higher forces, but the volume to surface area is too large for rapid cooling. Initial measurements on this wire and calculations on the actuator deflection showed that this wire would attain the required performance. See for instance Figure 3 for the force-temperature response of the wire. The measurements were performed on a 10kN MTS testing machine while measuring the wire's temperature with an infra red (IR) camera. The wires in the actuator were prestrained, slightly stressed and clamped at their ends. Holes were drilled in both ends of the actuator for entry into and exit from the channels for the air.

Implementation on Wind Turbines

The actuator can be implemented on a wind turbine blade in a number of forms. Firstly, it could be mounted as a flat extension to the trailing edge as done with piezo electric Thunder actuators by Gauna et al.(Bak et al., 2007). Secondly, the suction and pressure side of the existing profile could be replaced by the active surface as done by Lindroos et al. (Lindroos et al., 2008). Finally, the surface could be mounted near the trailing edge as a spoiler (Scott et al., 1997). This has a similar effect as microtabs (Standish and van Dam, 2005, Mayda et al., 2005), which are already under investigation for load control on wind

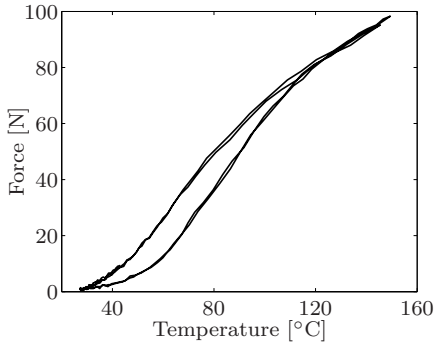

Figure 3: Force temperature response of the SmartFlex wire. The wire was prestrained 3%, fully restrained at its ends and heated by Joule heating.

turbines. See Figure 4 for schematic representations of the concepts discussed here on a DU96-W180 profile which is a common tip profile for wind turbines.

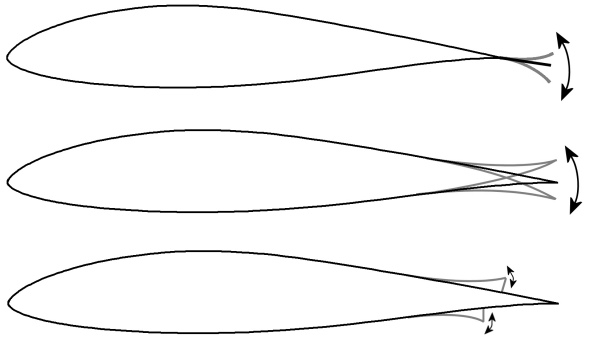

Figure 4: Possible implementation of a SMA actuator. From top to bottom: as extension to the trailing edge, as trailing edge wedge or active panels.

THERMAL CHARACTERISATION

The most important conceptual feature of the actuator is its increased cooling capacity in comparison with fully embedded wires. In order to make predictions about its behaviour and performance, the thermal behaviour was characterized. This was done by heating the wire to a certain temperature by Joule heating and subsequently cutting the power. The temperature decay was measured with an infra red (IR) camera and an exponential function $T = a \exp bt$ was fitted to the data, see Figure 5.
From the exponential decay the heat transfer could be calculated using basic heat equations (Bejan, 1993). The heat loss per unit length is given by:

$$q' = -hA(T_w - T_\infty) \tag{1}$$

With h being the heat transfer coefficient - the parameter of interest - A the circumference of the wire (or the surface area per unit length), T_w the temperature

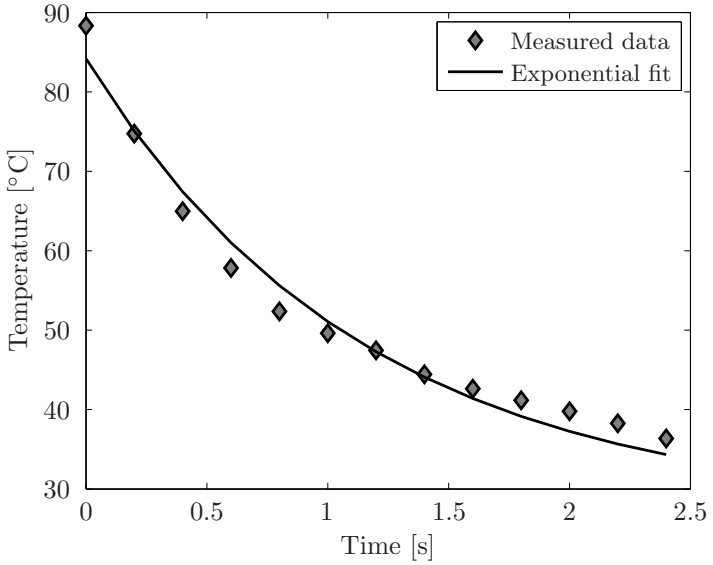

Figure 5: Example of exponential fit to the measured temperature data.

of the wire and T_∞ the temperature of the flow. In this case all experiments were conducted at room temperature. It was assumed that the flow did not heat up significantly when passing the wire because the air speed was very high. Consequently T_∞ remained constant. The temperature change as a result of the heat dissipation is defined as:

$$\frac{dT_w}{dt} = \frac{q'}{V\rho c_p} \tag{2}$$

In which, V is the cross-sectional area (or volume per unit length), ρ and c_p the density and heat capacity of the wire respectively. ρc_p was taken from (Boyd and Lagoudas, 1996) and good correspondence was observed with the measurements. The value can be obtained from the measurements when looking at the instant at which the wire starts heating up from T_∞. In this case the heat loss is zero and the relation between the input power and heat-up can be derived from equation 2, but with q' the generated heat through Joule heating, per unit length.
Combining equations 1 and 2 reads:

$$\frac{dT_w}{dt} = \frac{-hA(T_w - T_\infty)}{V\rho c_p} \tag{3}$$

This is a first order differential equation of which the solution reads:

$$T(t) = T_\infty + (T_0 - T_\infty)\exp\frac{-hA}{V\rho c_p}t \tag{4}$$

With T_0 the temperature at $t = 0$. In Table 1 the fits of the measured data can be seen. The resulting heat transfer coefficient is plotted in Figure 6.
Figure 6 and Table 1 indicate that the cooling of the wire is increased up to tenfold by active cooling. Moreover, the heat that is dissipated is quickly blown

Airflow [L/min]	a	b	h [W/Km^2]	R^2
0	95.6	-0.211	55	0.99
7	77.5	-1.01	260	0.99
11	85.2	-0.93	240	0.98
15	65.4	-1.38	356	0.98
18	69.9	-1.4	361	0.98
21	77.5	-1.62	417	0.97
23	81.8	-1.94	499	0.98
25	70.4	-2.28	587	0.97

Table 1: Exponential curve fit to the measured data.

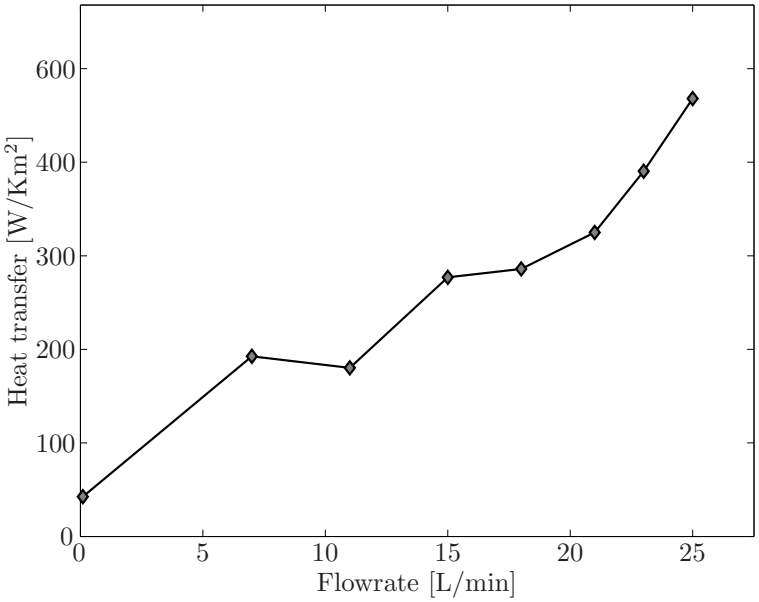

Figure 6: Measured heat transfer coefficient.

away, whereas it would have to be dissipated through the actuator in the case of a fully embedded wire. This build-up of heat would change the thermal boundary conditions of the wire and with it its response. This in sharp contrast with active cooling through forced convection in the channels. Additionally, the power consumption can be kept under control in comparison to externally mounted wires on a wind turbine, because the cooling can be switched off if the wire needs to be heated. The system therefore does not only have the potential to increase the actuation speed but also to increase the controllability.

CONTROLLER

Controllers for SMA actuated structures usually aim at tackling the hysteresis and non-linearities. Webb (Webb et al., 2000), for instance, uses the error between a reference signal and the actual displacement to update an adaptive hys-

teresis model to compute the actuation signal through a thermal model. Here, it was chosen to implement fuzzy logic control (Jantzen, 2007) to control the actuator. Ahn (Ahn and Nguyen, 2006) implemented a fuzzy logic supervisor to update the proportional, integration and derivative gain of a PID controller to perform displacement control with SMAs. Kumagai (Kumagai et al., 2006) used neural networks to train the fuzzy controller. Here, a fuzzy logic controller was heuristically tuned and it directly controlled the plant. The implementation of (direct) fuzzy logic was motivated by the non-linear characteristics of the system and the complexity of the set-up with its multiple controller outputs for only one degree of freedom of the plant (deflection of the actuator). The non-linearities arose from the non-linear behaviour of the SMA material, especially the hysteresis when going through actuation loops and the fact that the force and deflection flatten off at higher temperatures (see Figure 3). Secondly, the asymmetry of the temperature control system had to be taken into account. This asymmetry is caused by the different physical nature of the heating and cooling mechanisms. Heating is done by resistance heating, whereas cooling is attained by forced convection. Although forced convection is very effective in dissipating heat from the wire, it is still much slower than resistance heating in terms of attainable rate of temperature change $|dT/dt|$. Also, the inertia of the air leads to a delay between the control signal and the actual cooling. In this section relevant fundamentals and how fuzzy logic control was implemented on the system are discussed.

Fuzzy Logic Controller

With fuzzy logic control, three steps are executed to compute a control signal from the controller's input. See Figure 7.

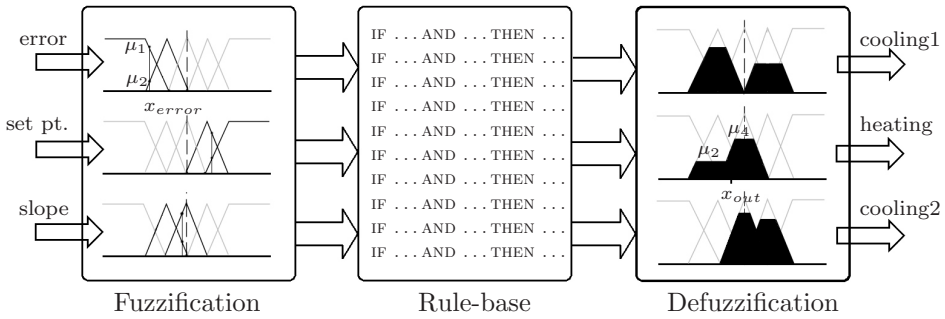

Figure 7: Scheme of the fuzzy logic controller, also indicating schematically how the different steps are implemented.

The three blocks in Figure 7 were implemented in the following way. First, the input of the actuator is converted to a value between 0 and 1 for different linguistic terms describing the state of the system; the so called degree of membership. For instance, a certain error input value x_{error} may lead to degrees of membership, indicated by μ_1 and μ_2 in Figure 7, of 0.4 for 'negative' and 0.7 for 'negative large'. This step is called fuzzification and the relation between

an input value and the degree of membership μ is described by membership functions, shown as triangular and trapezoid plots in Figure 7.
Here, the following input linguistic variables were chosen. The choice for the error signal is logical. It can be regarded as a proportional part of the controller and it was the error that was to be minimized. The deflection is important because it is related to stress, and thus to the temperature in the wire, which in turn determines the mechanical behaviour of the wire and says a great deal about its thermal behaviour. For instance, if the actuator is deflected to its fullest extent, it can be assumed that the wires on the compression side are very hot, which in turn would lead to rapid cooling when the heating is cut - even without forced convection. The slope of the set point is implemented because it determines the required speed of heating or cooling which is directly related to the required input power or valve set point. The number of inputs is limited because the number of rules in the rule base (and with it the computational time) increases exponentially with the amount of input parameters. Five linguistic terms and accompanying membership functions were defined for each input linguistic variable.
Subsequently, a rule-base is executed in which the occurrence of non-zero input membership grades is linked to an output fuzzy set through 'if-then' statements (second block in Figure 7). This linguistic approach of the rule base is very suitable for the kind of control that was sought. Because of the delay in cooling and the response of the SMA wire, smooth control of the cooling and actuating quickly with a heating signal over that cooling signal is wanted. The rule base controller makes it possible to minimize concurrent heating and cooling which limits the power consumption. Additionally, the controller was implemented in such a manner that still coupling between heating and cooling control is obtained. This is important to prevent jittering. Therefore, for instance, the rule base was chosen such that a dead zone exists around a zero error for the cooling.
Finally, a weighted average of the different results of the rule-base is computed using output membership functions, which forms the output of the controller. This is called defuzzification. For the heating signal seven linear (triangular and trapezoid) functions are used. For the valve output four output membership functions are defined: Three triangular functions and one singleton. The singleton is implemented through the rule base, such that it is executed when the opposite wire set is being heated and the side that is to be cooled is not. The goal is to prevent heat build-up in the actuator. The Center of Area method is used for computing the output value, meaning that the output signal is computed using the following relation (NI, 2009):

$$x_{out} = \frac{\int_{x_{\min}}^{x_{\max}} x f(x) dx}{\int_{x_{\min}}^{x_{\max}} f(x) dx} \tag{5}$$

Where $f(x)$ are the combined, activated output membership functions, x is the output parameter and $x_{\min}$ and $x_{\max}$ denote the domain over which x is defined. The Center of Area method is also schematically indicated in Figure 7. Three output signals are computed this way: a valve setting for each side

of the actuator and one power control signal for the current generators. The heating signal is split to wires on each side of the actuator, based on its sign. If the heating output is positive, power is fed to the wire set on one side of the actuator and if it is negative, to the other set. So there are four inputs to the plant, whereas the fuzzy controller only has three output linguistic parameters, see Figure 8. The power signal consists of voltage and current set points for the current generators which are adjusted for the change in electrical resistance due to the lattice transition from austenite and martensite or vice versa (Otsuka and Ren, 2005). On the other hand, for the cooling response, sometimes it is needed to cool both sets of wires at the same time. This also prevents the build-up of heat in the bender, which increases the controllability. Therefore two separate output signals for the cooling signals are needed.

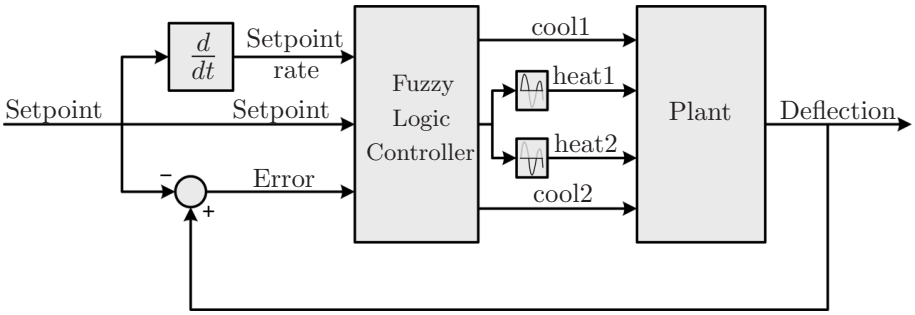

Figure 8: Control scheme for the fuzzy logic controller.

The controller was implemented on in LabVIEW 9.0 (National Instruments Netherlands BV, Woerden, The Netherlands). The digital-to-analogue and analogue-to-digital converters were National Instrument NI 9215 input and 9263 output modules on a NI cDAQ 9172 board. The control loop was executed at 50Hz.

Controller Performance

In order to investigate the performance of the controller separately from the actuator performance, an antagonistic set-up was built (See Figure 9). The set-up is schematically presented by the left side of Figure 2. In this case a laser target was mounted in the middle of a wire with 3% strain. To both sides of the target, electrodes and cooling channels, as intended on the actuator, were applied. This way, *de facto* two separately controllable wires were obtained. A laser displacement sensor was aimed at the laser target. This was used as the feedback signal. Heating the wire on one side, causes recovery of the strain in that part of the wire, simultaneously straining the other part further. Subsequent cooling of this side of the wire results in relaxation of the actuation force and simultaneous heating of the other side causes the laser target to move in opposite direction. The controller was manually tuned to the specific behaviour of the set-up and a series of tests was performed in which the target tracks a sinusoidal reference signal. The reference signal, the actual displacement and controller outputs were recorded. The performance of the actuator for a set point amplitude of 1.5mm and frequency of 0.6Hz can be seen in Figure 10.

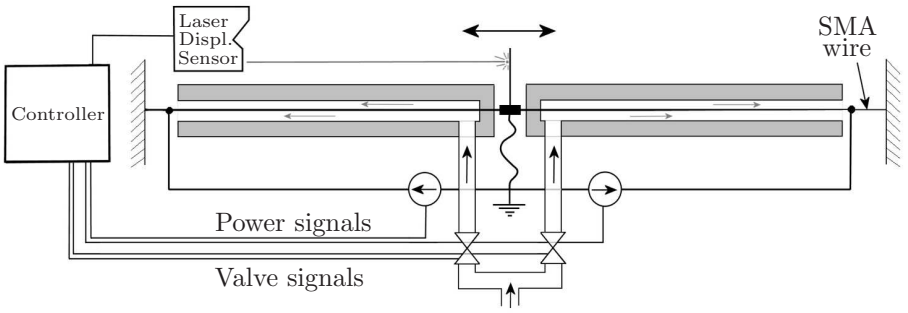

Figure 9: Schematics of the antagonistic set-up.

The figure shows that the response was as wanted: the wire that was not being heated, was cooled by a relative smooth signal. When the set point time derivative was at its maximum, the valve was opened slightly more. The heating signal response was much more irregular than the cooling response because the

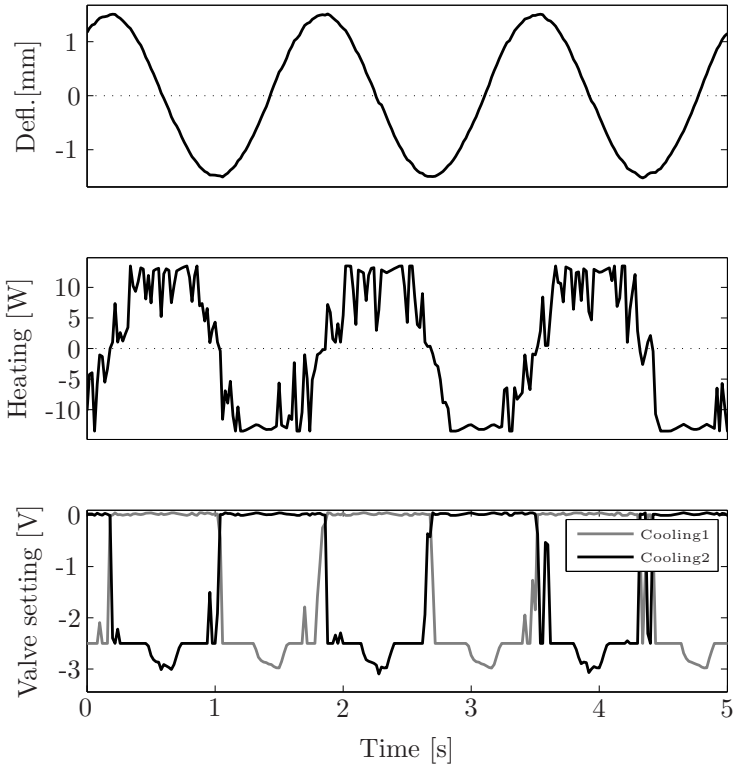

Figure 10: Response of the antagonistic set-up when tracking a set point with an amplitude of 1.5mm and 0.6Hz. From top to bottom: the deflection of the system, the heating and the cooling output of the controller.

controller mainly used the current generators to minimize the error. A series of experiments tracking sinusoidal reference signals with different amplitudes and frequencies was performed. The results of the tests are presented in several ways. First of all, the error between the reference signal and the actual displacement was plotted. See Figure 11.

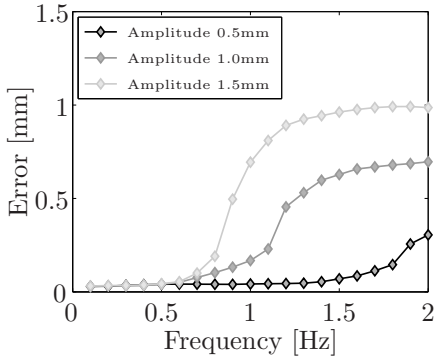

Figure 11: Error on the antagonistic set-up as a function of different amplitudes.

As expected, the controller failed in controlling the set-up for higher frequencies and amplitudes. But the error remained very small for all amplitudes up to 0.6Hz, which covers the frequency spectrum that is under consideration for large MW-sized wind turbines. However, when observing the nature of the response above 0.6Hz (See Figure 12), it was noticed that the error was caused by a reduction in amplitude and a phase delay while the response maintained a sinusoidal shape. Therefore, the transfer between the reference signal and the

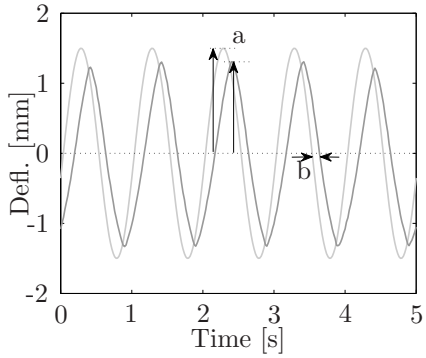

Figure 12: Time series of the antagonistic set-up tracking a sinusoidal reference signal. a) illustrates the difference ('transfer') between the amplitude of the set point signal and actual displacement. b) illustrates the phase change.

actual response of the signal can be presented in the form of a Bode plot of the closed loop system. See Figure 13.
As can be seen, the conclusions are similar as with the error plot of Figure 11: for higher amplitudes the cut-off frequency decreases. The closed loop system seems to perform as a third order system because the slope of the roll off is 60dB per decade. The bandwidth of the closed loop system, where it passes the

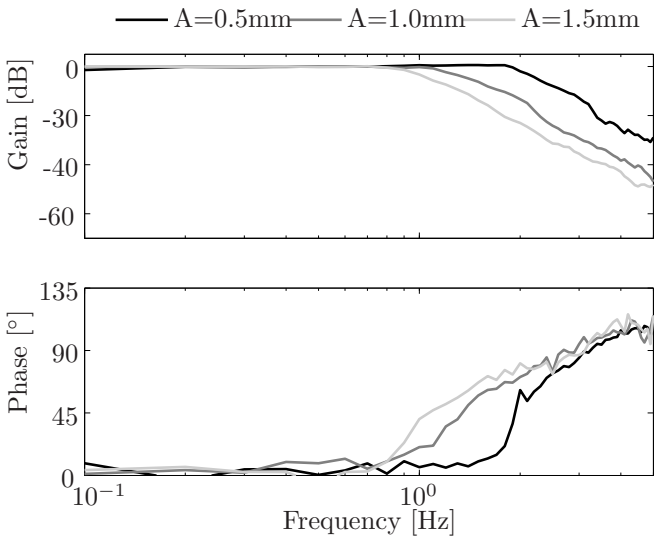

Figure 13: Bode-like plot of the antagonistic set-up for different amplitudes.

-3dB, seems to be at least 1Hz for all amplitudes. This knowledge can also be used to design a controller around the actuator system.

ACTUATOR TESTING

Once that the potential and controllability of the actuator system were shown experiments on the actual actuator were performed. To study its performance, a set of experiments was conducted of the same kind as on the antagonistic set-up. Because of the similar nature of the system (compare Figure 9 to Figure 14) the same controller structure was employed. The actuator is after all based on the same SMA wires and cooling channels and the wires were also applied in an antagonistic configuration. On the other hand, the SMA behaviour moves from a temperature-strain to a temperature-stress dominated controlled configuration because of the small strain fluctuations the SMA wire experiences in the actuator. Thus, the membership functions and rules had to be changed to accommodate for the different deflection behaviour of the actuator as compared to the antagonistic set-up. Moreover, the displacement of the 200mm long actuator is induced by bending, whereas the antagonistic set-up describes a translational movement. Thus, these tests also provided information about the dynamic response of the beam actuator, as compared to only the SMA and thermal behaviour as tested on the antagonistic setup.

Sinusoidal Reference Signal Tracking

The actuator was set to track a sinusoidal set point signal, with the displacement transducer aimed at the tip as feedback signal. In Figure 15 the response to a low frequency reference signal can be seen, including the control signals. The response and the control signals seemed to be symmetric and the tracking was

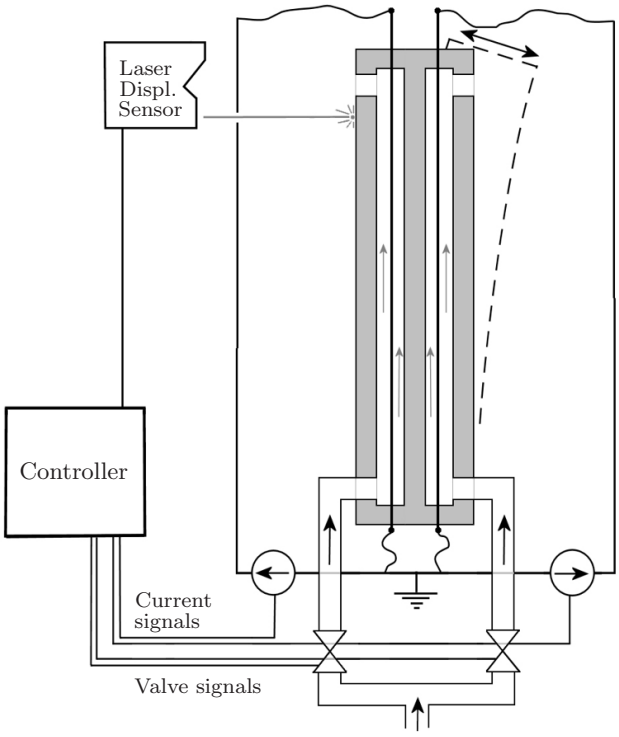

Figure 14: Schematics of the actuator test set-up.

fairly good. However, the power control was somewhat irregular, with high spikes. The execution of the singleton output membership function for the valves can be seen as the constant cooling signal of -2V when the deflection of the actuator is around its maximum.
For higher frequencies the actuator response is presented in Figure 16. As can be seen, the bender behaviour became increasingly unstable with increasing frequency. The actuation frequency was maintained, but the response was not sinusoidal; the actuator was jumping from side to side.
This was ascribed to snap-through behaviour around the neutral position of the bender which was caused by the room that the wires have in the channels. When the actuator moves through the neutral position, the wires move from one side of the channel to the other. See Figure 17. In addition, the wires may cut in the channel surface during actuation, but the polymer that is selected for the actuator is known for its good abrasive properties.
The sign of the moment that a wire exerts, does not change because the channel is on one side of the neutral axis of the actuator, but around the neutral axis there are two stable positions. This was also substantiated by looking at the quality of a fit of a sine ($a\sin(bt+c)$, where t is the time and a, b and c are the parameters that were fitted to the measured data). R^2, the square of the correlation between the measurement data and the fitted values, is plotted in Figure 18 for the response of the antagonistic set-up and the actuator. It is a

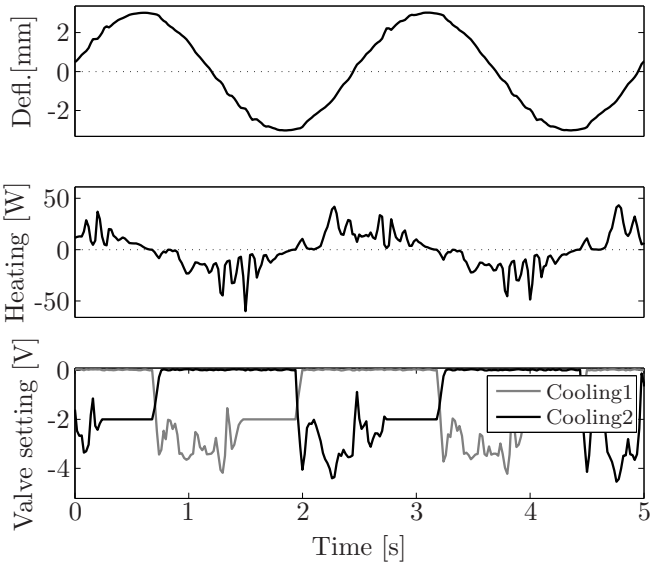

Figure 15: Response of the actuator to a 0.4Hz reference signal.

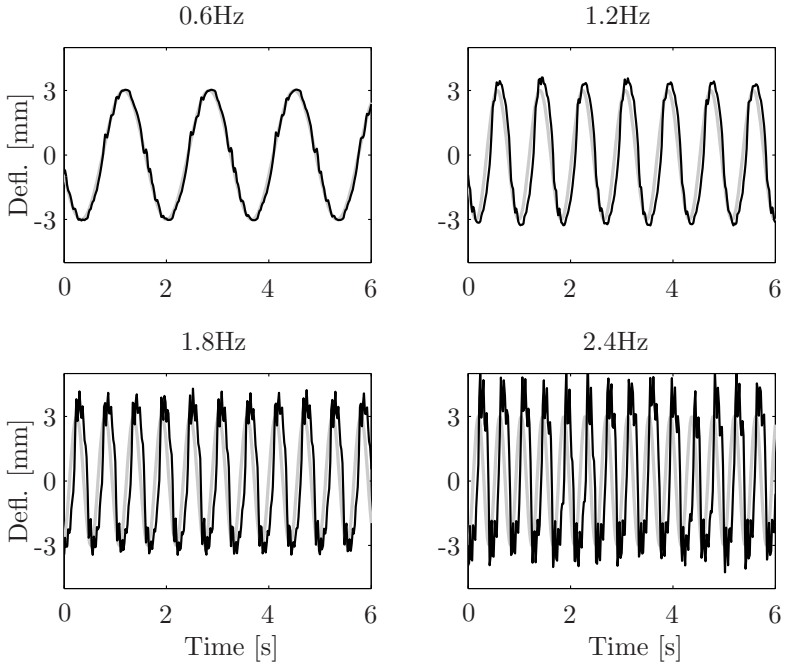

Figure 16: Performance of the bender in tracking sinusoidal signals with different frequencies all have an amplitude of 3mm. The set point is depicted in grey and the response in black.

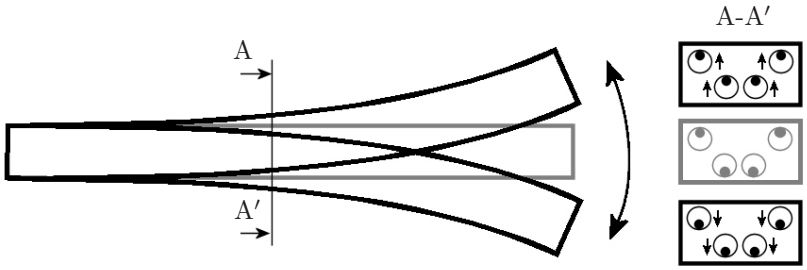

Figure 17: Schematic representation of the wires moving in their channels, causing an unstable neutral position (shown in grey).

measure for the quality of the fit. Here it indicates whether the signal remained a sinusoidal shape, even if tracking of the reference signal was lost. $R^2 = 1$ indicates a perfect sinusoidal response.

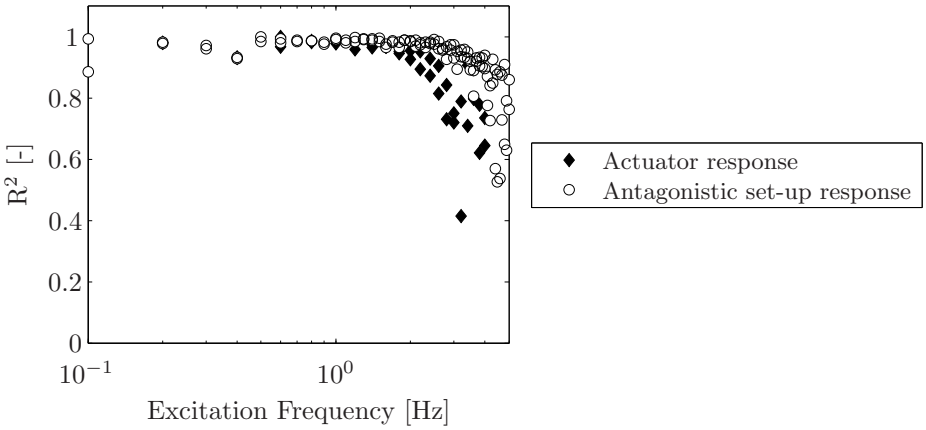

Figure 18: Square of the correlation for the response of the actuator and the antagonistic set-up

It can be concluded from the figure that the actuator response lost its sinusoidal shape at much lower frequencies than the antagonistic set-up. This can only be attributed to the specific beam dynamics because the SMA material and the control system were the same.

Composite Sinusoidal Reference Signal Tracking

Normally, the wanted deflection of the actuator, needed to counter blade vibrations, consists of a combination of different frequency components. To study the effect, a series of measurements on composite sinusoidal signals was performed. Moreover in such experiments it is also possible to see the response of the high frequency component with varying mean. The response and the set point for different frequency combinations are presented in Figure 19.
Here the snap-through behaviour, especially around the neutral position can also be seen in the form of jittering around the reference signal. The controller

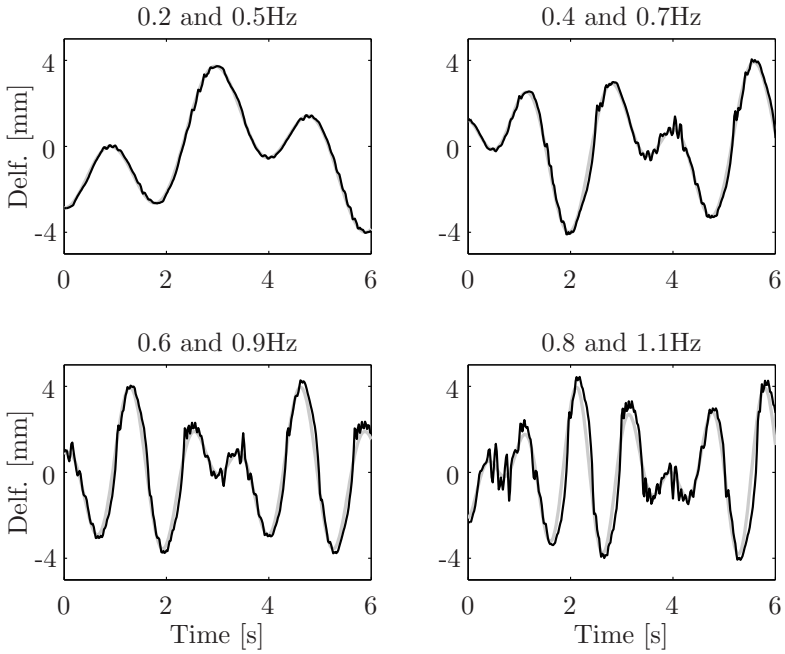

Figure 19: Performance in tracking composite sinusoidal signals of different frequencies. The reference signal is plotted in grey and the actual response in black.

was unable to minimize the error because the actuator position was unstable around zero deflection. When the reference signal was increased or decreased, tracking was restored again.

Step Response

Finally, the closed loop response to a step on the set point is presented. This was an interesting case because a sinusoidal reference signal posed a constantly varying signal, but with the response to a step, the system had to act quickly with a small overshoot. Because this required a different type of response of the controller, it was an interesting case to subject the system to. Figure 20 presents the response to a step of ±3mm.
The controller also seemed to perform well in this case. The wire set that is on the extension side is constantly cooled and the controller controls the actual position of the actuator through the heating signal. However, there was some overshoot and the response seemed to be asymmetric. Because the controller is completely symmetric, this has to be ascribed to the beam behaviour. Moreover, when a zoom of the steps is observed (see Figure 21), an acceleration of the deflection when it passes the neutral position between -1 and 1mm deflection, in both directions, can be seen. This can be attributed to the snap-through behaviour. Moreover, during the overshoot, a vibration is observed which has the same frequency of the first natural vibration of the actuator.

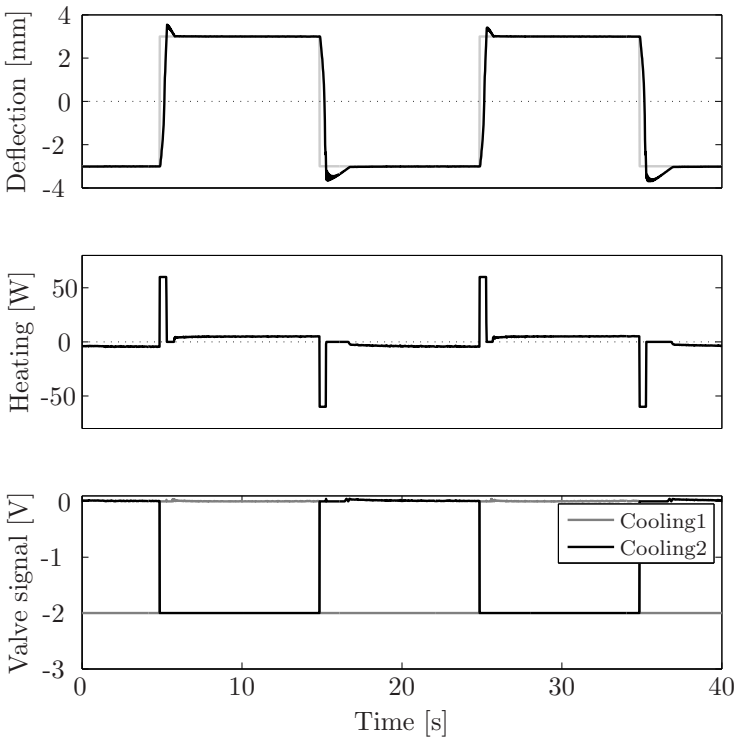

Figure 20: Response of the actuator to steps on the set point signal

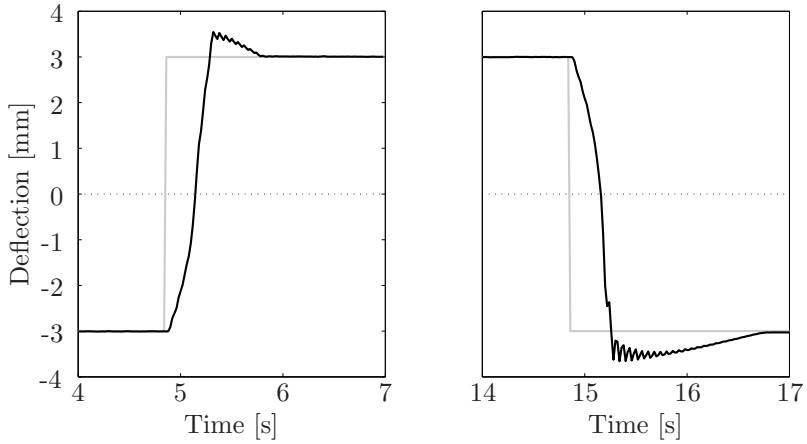

Figure 21: Zoom of the step response around the steps.

CONCLUSIONS AND DISCUSSION

Actuator performance

An actuator was designed and manufactured, aimed at serving as a morphing surface. The design specifically tackled the bandwidth issue, associated with the

dynamic use of SMA material to drive an actuator. From the thermal experiments we can conclude that the cooling channels, as they are intended in the actuator, greatly increases the cooling rate, up to ten times in comparison to the same set-up without forced convection. Moreover, the advantage of cooling via internal channels over external cooling is that the cooling rate can be controlled, limiting the power consumption and increasing the controllability because the dissipated heat is blown away and therefore there is no heat build-up in the actuator.
To study the performance of the bender a fuzzy logic controller was designed because of the non-linearities involved in the bender and the SMA material, and because of the linguistic nature that the controller offers. Tests with the actuator showed that a reference signal up to 0.6Hz could be tracked, which covers a large part of the load spectrum associated with MW-sized turbines.
For implementation as an actual flap several design improvements will have to be made, mainly regarding the shape of the cooling channels. Now the channels are relatively high as compared to the thickness of the actuator. In order to keep the channels on their respective side of the neutral axis, a thick actuator was constructed. This, however, limits the deflection of the actuator because its stiffness increases faster than the moment arm of the wire.
It is asserted that a feedback controller is needed to control the actuator, especially if it is to be subjected to external loading. However, further characterisation and modelling efforts will increase the controller's performance.

Conclusions on implementation on wind turbines

Although the influence of the temperature of the cooling gas used to cool the SMA wires is a parameter that has not been studied here, it has an influence on the performance of the actuator. The cooling process is forced convection, and its performance depends principally on four different parameters: The mass of the SMA wires, the flow rate of the gas, their respective specific heat capacities and the difference of temperature between the wires and the fluid. The latter may change with the seasonal conditions, but, if needed, chilled air may be applied or use of the Joule-Thomson effect can be made.
Another issue with large scale application of SMA material as actuator is the power consumption. Evaluation of the electrical power, which is an output of the fuzzy logic controller, has been made and within the frequency range of interest the maximum average power consumption is 20W per centimeter actuator width. Moreover, Andersen *et al.* (Andersen et al., 2010) made an analysis of load reduction potential as function of the fraction of the span on which load control devices are applied. They found 34% fatigue load reduction with 12.6m span equipped with flaps on a 5MW turbine with 60m long blades that was also under consideration here. For higher flap widths, the added load reduction potential was low. This 12.6m flap width constitutes a power consumption of 25kW per blade for the SMA actuator discussed here, which equals 1.5% of the rated power for application of the morphing surface on all three blades. Finally, although this research was aimed at obtaining a morphing surface for aerodynamic load control on wind turbines, the actuator concept could also be applied to any similar application requiring $\sim$1Hz actuation.

ACKNOWLEDGMENTS

This research was supported by the European Commission's UpWind program and performed within the Delft University of Technology's wind energy research institute DUWIND.

References

K.K. Ahn and B.K. Nguyen. Position control of shape memory alloy actuators using self tuning fuzzy pid controller. *International Journal of Control, Automation, and Systems*, 4:756–762, 2006.

P.B. Andersen, L. Henriksen, M. Gaunaa, C. Bak, and T. Buhl. Deformable trailing edge flaps for modern megawatt wind turbine controllers using strain gauge sensors. *Wind Energy*, 13:193–206, 2010.

C. Bak, M. Gaunaa, P.B. Andersen, T. Buhl, P. Hansen, K. Clemmensen, and R. Moeller. Wind tunnel test on wind turbine airfoil with adaptive trailing edge geometry. In *Proc. of the 45th AIAA Aerospace Science Meeting and Exhibit*, January 2007. AIAA-2007-1016.

S. Basualdo. Load alleviation on wind turbine blades using variable airfoil geometry. *Wind Engineering*, 29(2):169–182, 2005.

A. Bejan. *Heat transfer*. John Wiley and sons, 1993.

E. A. Bossanyi. Wind turbine control for load reduction. *Wind Energy*, 6: 229244, 2003.

J.G. Boyd and D.C. Lagoudas. Physical metallurgy of TiNi-based shape memory alloys. *International Journal of Plasticity*, 12:805–842, 1996.

T. Buhl, M. Gaunaa, and C. Bak. Potential load reduction using airfoils with variable trailing edge geometry. *Journal of Solar Engineering*, 127:503–516, 2005.

C. J. Doran. The effect of prestrain on the actuation performance of embedded shape memory alloy wires. In *Proc. of second European Conference on Smart Structures and Materials*, 1994.

B. Enenkl, V. Kloppel, D. Preiler, and P. Janker. Full scale rotor with piezoelectric actuated blade flaps. In *Proc. of the 28th European Rotorcraft Forum*, 2002.

L. Fumagalli, F. Butera, and A. Coda. Smartflex niti wires for shape memory actuators. *Journal of Materials Engineering and Performance*, 18:691–695, 2009.

M. Gaunaa. Unsteady two-dimensional potential-flow model for thin variable geometry airfoils. *Wind Energy, Special Issue: Smart Blades*, 13(2-3):167–192, 2010.

S.R. Hall and E.F. Prechtl. Development of a piezoelectric servoflap for helicopter rotor control. *Smart Materials and Structures*, 5:26–34, 1996.

D. A. Hebda, M. E. Whitlock, J. B. Ditman, and S. R. White. Manufacturing of adaptive graphite/epoxy structures with embedded nitinol wires. *Journal of Intelligent Material Systems and Structures*, 6:220–228, 1995.

J. Jantzen. *Foundations of Fuzzy Logic Control*. John Wiley and sons, 2007.

S. Joncas, O. Bergsma, and A. Beukers. Power regulation and optimization of offshore wind turbines through trailing edge flap control. In *Proc. of the 43rd AIAAAerospace Science Meeting and Exhibit*, January 2005. AIAA-2005-394.

J. Jonkman, J. Johansen, and K. Lindenburg *et al.* Description of the UpWind reference wind turbine - version 9. Technical report, UpWind Integrated Project, 2007.

A. Kumagai, T.I. Lui, and P. Hozian. Control of shape memory alloy actuators with a neuro-fuzzy feedforward model element. *Journal of Intelligent Manufacturing*, 17:45–56, 2006.

D.C. Lagoudas, editor. *Shape Memory Alloys - Modeling and Engineering Applications*. Springer, 2008.

T. Lee and I. Chopra. Design of piezostack-driven trailing-edge flap actuator for helicopter rotors. *Smart materials and structures*, 10:15–24, 2001.

T. Lindroos, M. Sippola, and J. Koskinen. The application of smart structures for large wind turbine rotor blades. In *56th IEA Topical Expert Meeting*, pages 167–178, May 8-9 2008.

E.A. Mayda, C.P. van Dam, and D. Yen Nakafuji. Computational investigation of finite width microtabs for aerodynamic load control. In *Proc. of the 43rd AIAAAerospace Science Meeting and Exhibit*, January 2005. AIAA-2005-1185.

NI. *LabVIEW - PID and Fuzzy Logic Toolkit User Manual*. National Instruments, June 2009.

K. Otsuka and X. Ren. Physical metallurgy of tini-based shape memory alloys. *Progress in Materials Science*, 50:511–678, 2005.

J.K. Rice and M. Verhaegen. Robust and distributed control of a smart blade. *Wind Energy*, 13(2):103–116, 2010.

L. Saggere and S. Kota. Static shape control of smart structures using compliant mechanisms. *AIAA journal*, 37(5):572–578, 1999.

R.C. Scott, S.T. Hoadley, C.D. Wieseman, and M.H. Durham. The benchmark active controls technology model aerodynamic data. In *AIAA, Aerospace Sciences Meeting and Exhibit*, 6-9 Jan 1997. AIAA-1997-829.

S. G. Shu, D. C Lagoudas, D. Hughes, and J. T. Wen. Modeling of a flexible beam actuated by shape memory alloy wires. *Smart Materials and Structures*, 6:265, 1997.

K. Singh, J. Sirohi, and I. Chopra. An improved shape memory alloy actuator for rotor blade tracking. *Journal of Intelligent material systems and structures*, 14(12):767–786, 2003.

G. Song, P. Lam, T. Srivatsan, B. Kelly, and B. Agrawa. Application of shape memory alloy wire actuator for precision position control of a composite beam. *Journal of Materials Engineering and Performance*, 9:330–333, 2000.

K.J. Standish and C.P. van Dam. Computational analysis of a microtab-based aerodynamic load control system for rotor blades. *Journal of the American Helicopter Society*, 50(3):249–258, 2005.

K. van Rijswijk. *Thermoplastic composite wind turbine blades: vacuum infusion technology for anionic polyamide-6 composites*. PhD thesis, Delft University of Technology, 2007.

J. van Wingerden. *Control of Wind Turbines with Smart Rotors: Proof of Concept & LPV Subspace Identification*. PhD thesis, Delft University of Technology, 2008.

J. van Wingerden, A.W. Hulskamp, T. Barlas, B. Marrant, G. van Kuik, D.-P. Molenaar, and M. Verhaegen. On the proof of concept of a smart wind turbine rotor blade for load alleviation. *Wind Energy*, 11:265–280, 2008.

G. Webb, L. Wilson, D. Lagoudas, and O. Rediniotis. Adaptive control of shape memory alloy actuators for underwater biomimetic applications. *AIAA journal*, 38:325–334, 2000.

G. Zhou and P. Lloyd. Design, manufacture and evaluation of bending behaviour of composite beams embedded with sma wires. *Composites Science and Technology*, 69:2034–2041, 2009.